Reentrant quantum phase transitions in two capacitively coupled Josephson arrays in perpendicular magnetic fields

Guillermo Ramírez-Santiago
Departamento de Física-Química, Instituto de Física, Universidad Nacional Autónoma de México, Apartado Postal 20-364, México, 01000, Distrito Federal, Mexico

Jorge V. José
Department of Physics, Fronczak Hall, University at Buffalo, State University of New York, Buffalo, New York 14260-1500, USA
(Received 30 July 2007; published 21 February 2008)

We have studied the phase diagram structure of two capacitively coupled Josephson junction arrays as a function of their charging energy E_c, Josephson coupling energy E_J, and a homogeneous perpendicular magnetic field. The arrays are coupled via a site interaction capacitance, $C_{\text{int}}=C_{\text{inter}}/C_m$, with C_{inter} as the interlayer mutual capacitance and C_m as the intralayer mutual capacitance defined as the nearest neighbor grain mutual capacitance. The parameter that measures the competition between thermal and quantum fluctuations in the ith array ($i=1,2$) is $\alpha_i \equiv E_{c_i}/E_{J_i}$. The phase structure of the system is dominated by the thermally induced and magnetically induced vortices as well as intergrain charge induced excitations. We have studied the capacitively coupled array behavior when one of them is in the vortex dominated regime, and the other in the quantum charge dominated regime. We determined the different possible phase boundaries by carrying out extensive quantum path integral Monte Carlo calculations of the helicity modulus $\Upsilon_{1,2}(\alpha,f)$ and the inverse dielectric constant $\epsilon_{1,2}^{-1}(\alpha,f)$ for each array as a function of temperature, interlayer capacitance C_{int}, quantum parameter α, and frustration values $f\equiv\frac{\Phi}{\Phi_0}=1/2$ and $f=1/3$. Here, Φ is the total flux in a plaquette and Φ_0 is the quantum of flux. We found an intermediate temperature range when array 1 is in the semiclassical regime ($\alpha_1=0.5$) and array 2 is in the quantum regime with $1.25\leqslant\alpha_2<2$, in which $\Upsilon_2(T,\alpha,f=1/2)>0$ and then goes down to zero while $\varepsilon_2^{-1}(T,\alpha,f=1/2)$ increases from zero up to a finite value. This behavior is similar to the one previously found for unfrustrated capacitively coupled arrays. However, for $\alpha_2=2.0$, *a reentrant transition* in $\Upsilon_2(T,\alpha,f=1/2)$ occurs at intermediate temperatures for $C_{\text{int}}=0.782\,61$, 1.043 48, and 1.304 35. For smaller values of the interlayer capacitance no phase coherence was found in array 2. This suggest that the increase between the array capacitive coupling induces a normal-superconducting-normal (N-SC-N) reentrant phase transition. For values of $\alpha_2>2.0$, the quantum array only exhibits an insulating phase, while the semiclassical array shows a superconducting behavior. In contrast, for phase frustration, $f=1/3$, we found that when array 2 is in the full quantum regime, $2\leqslant\alpha_2\leqslant4$, the semiclassical array is the one that shows a reentrant N-SC-N behavior at relatively low temperatures. This reentrance in the coupled array behavior is a manifestation of the *gauge invariant capacitive interaction* and the duality relation between vortices, in the semiclassical array, and charges in the quantum-fluctuation dominated array. We find that the phase diagrams for $f=1/2$ and $f=1/3$ are very different in nature.

DOI: 10.1103/PhysRevB.77.064513 PACS number(s): 74.81.Fa, 03.75.Lm, 73.43.Nq, 05.10.Ln

I. INTRODUCTION

Josephson junction arrays (JJAs) have been an important laboratory for experimentalists and theorist and for applications. Recently, small JJAs have been used to construct a 16 qubit quantum computer.[1] This system is capable of carrying out fast computations and could eventually be used in wide practical applications. The combination of classical and quantum regimes can be studied simultaneously in capacitively coupled JJAs that allow for new parameter regimes to be studied where further applications can be uncovered. In this paper, we consider such a system in the presence of external homogeneous magnetic fields. Magnetic fields play an important role in the JJA responses and properties. Small JJAs also offer the opportunity to explore and study phase transitions driven by thermal and/or quantum fluctuations. For more than two decades, two-dimensional JJAs have been the focus of extensive studies from the theoretical[2–29,31–34] as well as from the experimental points of view.[35–47] Advances in submicrometer technology[41,42] and in nanolitographic techniques[43,44] have allowed to produce relatively large arrays made of ultrasmall superconductor-insulator-superconductor JJA. The junction areas may vary from a few microns to submicron dimensions, with self-capacitances on the order of $C_s\approx3\times10^{-2}$ fF and nearest neighbor mutual capacitances $C_m\approx1$ fF. Note that the mutual capacitance can be at least 2 orders of magnitude larger than the self-capacitance. In these arrays, there are two competing energies: the Josephson coupling energy E_J and the charging energy $E_C=(2e)^2/(2C_m)$ of the junctions, with e as the electron charge. The former is associated with Cooper pairs tunneling between neighboring superconducting (SC) island. The latter is connected with the electrostatic energy necessary to add one Cooper pair in one of the junction islands that can lead to charge localization. A homogeneous external magnetic field can induce frustration effects in the phases of the superconducting order parameter of the array's junctions. A gate voltage in turn can produce *charge frustration*. A combina-

tion of both frustrations can lead to very interesting complex phenomena. An important prediction for certain magnetic to charge frustration ratios is that the JJA may be in a quantum Hall phase.[34,48–50]

In this paper, we discuss the phase behavior of micron size Josephson junctions in two capacitively coupled arrays in the presence of uniform perpendicular magnetic fields. These magnetic fields nucleate magnetic vortices in the arrays that lead to a uniform magnetic frustration. At fractional rational values of the index of frustration, $f \equiv \frac{\Phi}{\Phi_0} = p/q$, with p and q as prime numbers, the magnetic vortices form a commensurate lattice to the underlying junction network lattice. The JJA Hamiltonian is periodic in the frustration index f with period $f=1$; one needs to consider then only the frustration range $0 < f \leqslant 1/2$. Near fractional rational values of f, topological defects from the ordered lattice—excess single vortices or domain wall excitations—determine the array phase behavior at finite temperatures. A domain wall is a topological excitation that separates two ground states that cannot be converted into each other by a continuous transformation. One expects rich phase critical behaviors at finite temperatures due to the competition of the following topological excitations: (i) magnetic vortices, (ii) domain walls, (iii) thermally excited vortices, vortex pairs, and (iv) charge excitations.

We have used a path integral Quantum Monte Carlo algorithm to study the thermodynamic phase structure of two capacitively coupled and frustrated JJAs. We calculated the T versus α_i different phase diagrams from the vortex helicity modulus Υ_i and the charge inverse dielectric constant ϵ_i^{-1}. These quantities were evaluated as a function of temperature, quantum parameter α_i, array capacitive coupling, and frustration index f. We found that as the α_i capacitive coupling between the arrays and f vary, there are different scenarios in which *novel* reentrant phase transitions can appear in the Υ_i and ϵ_i^{-1} behaviors. These quantities are nonzero in the ordered phase (superconducting or insulating phases) and they usually go down to zero in the disordered phases (normal or conducting). There are, however, situations in the ordered phase that as the temperature is further lowered, Υ_i or ϵ_i^{-1} can exhibit a decrease down to zero. When this happens, the system undergoes a "reentrant" phase transition. The system returns to a disorderedlike phase, except that in this case, it is at low temperatures. In our case, the reentrances indicate transitions between superconducting to normal (SC-N), superconducting to insulating (SC-I), and insulating to normal (I-N) phases. Before we discuss the nature of our results, let us briefly review the general properties and features of a single classical JJA in a square lattice with an $f=p/q$.

A uniformly frustrated classical JJA has a discrete Z_q symmetry and the underlying continuous X-Y $U(1)$ symmetry. The existence of these discrete q symmetries leads to the possibility of having long-range order that can change the phase transition nature of the system. The ground state consists of a checkerboard vortex configuration with a $p \times q$ elementary cell. Of particular interest is the $f=1/2$ case when the phases of the array are fully frustrated.[51–53] For this frustration value, the current flows in each plaquette either clockwise (vortex strength $+1/2$) or counterclockwise (vortex strength $-1/2$) leading to a discrete Z_2 chiral symmetry. From this ground state vortex configuration, one expects the system to develop an Isinglike ordering. However, results of extensive finite temperature studies and analysis indicate that the nature of the phase transitions in the classical fully frustrated JJA is different from the one expected only from ground state symmetries. For instance, it has been shown that the Z_2 transition is not in the same universality class as the two-dimensional (2D) Ising transition and that the $U(1)$ jump in the helicity modulus is larger than the universal jump in the pure XY model.[51–56,56,58–60] A detailed analysis of the topological excitations in the fully frustrated system shows that its behavior is analogous to that of the XY-Ising model.[61]

For frustration $f=1/3$, in addition to the $U(1)$ continuous symmetry, the JJA model has a $Z_3 \times Z_2$ symmetry that leads to a sixfold degeneracy of the ground state vortex configuration. It has been shown that the domain wall energy between three ground states in the same class is different from that corresponding to two ground states that belong to different classes.[57] This leads to the possibility of three different types of phase transitions: the first one is related to the proliferation of domain walls between three ground states connected by the Z_3 symmetry, the second one due to fluctuations between two types of ground states connected by the Z_2 symmetry, and the third one due to the continuous $U(1)$ symmetry leading to the dissociation of vortex-antivortex pairs. Results from classical microcanonical Monte Carlo (MC) calculations led to the conclusion that the transition temperatures occur in the following order, $T_{U(1)} < T_{Z_2} < T_{Z_3}$.[57] The low-temperature charge configurations were calculated for the charge filling ratio f_c—with f_c in between $(1/3, 1/2)$. On the other hand, the low-temperature charge configurations of the Coulomb gas on a square lattice for the charge filling ratio f_c in the range $1/3 < f < 1/2$ were obtained from Monte Carlo simulations.[62] Two separate transitions were found at temperatures T_p and T_{Coul} with $T_p < T_{\mathrm{Coul}}$. The charge configurations were arranged as periodic combinations of a few basic stripped patterns characterized by partially filled diagonal paths. The freezing of charges within these paths lead to the a low-temperature phase transition at temperature T_p, which sensitively depends on the value of $f_c = p_0/q_0$ within those paths. At higher temperatures, a Berezinskii-Kosterlitz-Thouless transition takes place at the temperature T_{Coul}. This transition is related to the unbinding of charge dipoles.

For micron sized Josephson junctions, the charging energy E_C can be larger than the Josephson coupling energy E_J and the thermal energy $k_B T$ (k_B is the Boltzmann constant), so that quantum effects become important. A Josephson array with these parameters will be denoted as a quantum Josephson array (QJJA). In the semiclassical limit, $E_J \gg E_C$, the phase of the superconducting order parameter of the junctions is well defined. The Josephson coupling induces fluctuations in the charge number that leads to a supercurrent and the average Cooper pair number is undefined. In this regime, the thermal vortex excitations are pinned by the intrinsic lattice potential and the array as a whole behaves as a superconductor. In the quantum limit, $E_J \ll E_C$, the electric field localizes the Cooper pairs in the islands and the quantum fluctuations of the superconducting order parameter delocal-

ize the thermally induced vortex excitations. This charge localization in the junction islands drives the array to an insulating phase. In this regime, the relevant topological excitations are the charges. The number of Cooper pairs $\hat{n}$ and the phase of the superconducting order parameter $\hat{\phi}$ are quantum conjugate variables which satisfy the Heisenberg's uncertainty relation[64] $\Delta\hat{n}\Delta\hat{\phi} \geq 1/2$. The transition from insulator to superconductor depends on the JJA relevant parameters such as the self-capacitance and mutual capacitance between the junctions, the charging energy, the temperature, and the presence of offset charges and/or external magnetic fields. There has been a significant effort to study and better understand the T versus $\alpha = E_c/E_J$ phase diagram of the QJJA. It has been shown that for a two-dimensional JJA, the phase diagrams may exhibit a rich phase structure.[65,66] To unravel the physics of this interesting system, several approaches have been used: mean field theory,[2–4,12,15,16,26] renormalization group techniques,[5,6,23] mapping of the QJJA model Hamiltonian onto other statistical models,[24,25,27,28,33] and quantum Monte Carlo calculations.[7–9,20,22,23,72] Nonperturbative analyses of this model and its connections to planar Chern-Simons gauge theories have also been analyzed.[34,73,74] Recently, QJJAs have also been studied within the context of quantum phase transitions.[27,28,63]

Experimental studies of the SC-I phase transition, induced by the charging energy as a function of α, were carried out by groups in Delft[39] and Harvard.[40] In these experiments, the junction sizes were constant, while they varied the normal state junction resistance to change the Josephson coupling energy. This allowed them to fabricate arrays with α in the range 0.13–4.55 (Ref. 39), or as high as 33.[40] The JJAs have the advantage, over films, that their geometric structure can be carefully controlled during fabrication. Another experiment[43] analyzed a 2D array of resistively shunted small Al-AlO_x-Al Josephson junctions. They found that for large values of the junction resistance and large charging energies, an I-SC transition was present when the shunt resistance became smaller than the quantum of resistance, $2h/4e^2 = 6.45$ K Ω. The measured phase diagram was consistent with quantum-fluctuation-driven and dissipation-driven phase transition theories. For a comprehensive review and literature which has studied the phase transition properties of ultrasmall 2D JJAs, see Ref. 41. When magnetic frustration is added to the superconducting order parameter phases of an ultrasmall JJA, its behavior becomes even more complex. In addition to the vortex and charge excitations of the classical unfrustrated array, one needs to consider magnetic induced vortices (fluxons) and the associated domain wall excitations, as discussed above. One expects then to obtain a rich phase diagram due to the competition of the four different types of topological excitations: magnetic vortices, domain walls, thermally induced vortex pairs, and charge excitations.

A experimental system composed of *two capacitively coupled JJAs* made of ultrasmall junctions was discussed in a paper by the Delft's group[42] some time ago. Each array was produced with different α_i $(i=1,2)$ parameters. Theoretical studies of this system have been published in papers.[25,67–75] One of the most interesting configurations of these capacitively coupled arrays has one array in the quasiclassical regime $(\alpha_1 \leqslant 1.5)$ and another is in the quantum regime $(\alpha_2 > 1.5)$. The semiclassical vortices in array 1 and the quantum induced charges in array 2 are simultaneously well defined variables. In this case, vortices and charges interact via a gauge field with strength controlled by the interlayer capacitance.[71] This peculiar interaction resembles the composite fermion scenario of the fractional quantum Hall effect. Nonetheless, the physical realization of those interactions is completely different from that one seen in a single JJA. Charge frustration effects in the capacitively coupled two-dimensional JJA layers have also been analyzed.[25] The corresponding Hamiltonian was mapped into the $\mathbf{S}=1$ and the $\mathbf{S}=1/2$ anisotropic XYZ antiferromagnet near the particle-hole symmetry line and the maximal frustration line, respectively. It was shown that near the maximal frustration line, the system may exhibit a quantum phase transition from charge-density waves to a supersolid phase displaying both diagonal and off-diagonal long-range orders. The dynamic and transport vortex parameters at $T=0$ of the capacitively coupled JJA with phase and charge frustration have also been analyzed.[73] There, it was shown that the vortex Hall conductivity in each layer and the Hall drag conductivity between the layers were quantized. The longitudinal vortex conductivity shows a perfect drag effect giving rise to two equally large but opposite currents in each of the layers. A Ginzburg-Landau approach to study the topological excitations captures the following phases: the superconducting and insulating phases and the novel quantum Hall phase due to the condensation of composite electric and magnetic excitations.[74,75]

In a recent study,[72] we carried out extensive quantum path integral Monte Carlo calculations to obtain the phase diagram of this interesting system in zero magnetic field (Paper I). We found a series of phase and charge reentrant phase transitions when one array was in the semiclassical limit and the other was in the quantum regime, for different values of the two array capacitive coupling. In this paper, we extend our studies to the nontrivial case when a uniform magnetic field introduces frustration in the junction phases and calculate the phase diagram structure of the system.

The Hamiltonian describing the coupled arrays can be formally written as $\hat{\mathcal{H}} = \hat{H}_J(1) + \hat{H}_J(2) + \hat{H}_C(1,2)$. Here, $\hat{H}_J(i)$ denotes the Josephson Hamiltonians for each array. $H_C(1,2)$ denotes the two array capacitive interactions. $\hat{H}_J(i)$ contains a frustration phase shift, $2\pi f_{i,j} \equiv \int_i^j \vec{A}\cdot\vec{dl}/\Phi_0$. $H_C(1,2)$ includes the total charging energy matrix, including the self-capacitive and mutual capacitive terms, C_s, C_m, respectively, in each plane, plus the two array capacitive interactions. Notice that the magnetic field produces frustration in the phases of the superconducting order parameter only. Each array is characterized by the energy ratio $\alpha_i = E_{C_i}/E_{J_i}$ $(i=1,2)$, with the mutual array capacitive coupling $C_{\rm int}$, measured by the ratio of the interlayer self-capacitance $C_{\rm inter}$ to the intralayer mutual capacitance C_m, that is, $C_{\rm int} = C_{\rm inter}/C_m$. In the $\alpha_i \ll 1$ limit, the ith array is dominated by localized thermal vortex excitations V_i, while the Cooper pair excess charge excitations Q_i are in a superconducting state. In the $\alpha_i \gg 1$ regime, the system has the Q_i's localized yielding an insulating state, while the V_i's are delocalized. There are different parameter

regimes that can be studied. Here, we consider, as in Paper I,[72] the case when one array is V dominated, and the other one Q dominated. We vary the interaction strength between the vortex dominated array and the charge dominated array by changing the interlayer capacitive coupling $C_{\rm int}$. It is important to emphasize that the parameter values we used in our numerical calculations correspond to those of the experimental samples fabricated and studied at Delft.[39]

The outline of the paper is as follows. In Sec. II, we briefly define and explain the model and the path integral formalism used to evaluate its partition function. Next, we discuss the physical quantities calculated to characterize the phase transition structure of the model. In Sec. III, we present and discuss our results. Finally, in Sec. IV, we summarize our main findings and present our conclusions.

II. PATH INTEGRAL REPRESENTATION OF THE MODEL

In this section, we define the model Hamiltonian that describes two JJAs made of ultrasmall junctions capacitively coupled at each lattice site. We also write down the path integral representation of the partition function and the physical quantities to be calculated.

The model Hamiltonian is defined by[71]

$$\hat{\mathcal{H}} = \frac{Q^2}{2}\sum_{\langle \vec{r}_1,\vec{r}_2\rangle}\sum_{\mu=1,\nu=1}^{2}\hat{\mathbf{n}}_\mu(\vec{r}_1)\tilde{\mathbf{C}}^{-1}_{\mu,\nu}(\vec{r}_1,\vec{r}_2)\hat{\mathbf{n}}_\nu(\vec{r}_2) + E_{J_1} \times \sum_{\langle \vec{r}_1,\vec{r}_2\rangle}\{1-\cos[\hat{\phi}_1(\vec{r}_1)-\hat{\phi}_1(\vec{r}_2)-2\pi f(\vec{r}_1,\vec{r}_2)]\} + E_{J_2} \times \sum_{\langle \vec{r}_1,\vec{r}_2\rangle}\{1-\cos[\hat{\phi}_2(\vec{r}_1)-\hat{\phi}_2(\vec{r}_2)-2\pi f(\vec{r}_1,\vec{r}_2)]\}, \quad (1)$$

where the sums are over nearest neighbors, and μ and ν label the matrix elements of the mutual capacitive interactions. The vectors $\vec{r}_1$ and $\vec{r}_2$ denote the positions of the junctions in arrays 1 and 2, respectively. The Cooper pair operator is $\hat{\mathbf{n}}_\mu(\vec{r}_1)$, and the phase operator for the superconducting order parameter is $\hat{\phi}_\nu(\vec{r}_2)$. Since $\hat{\mathbf{n}}_\mu$ and $\hat{\phi}_\nu$ are conjugate variables, the Heisenberg commutation relation $[\hat{\mathbf{n}}_\mu(\vec{r}_1),\hat{\phi}_\nu(\vec{r}_2)] = -i\delta_{\vec{r}_1,\vec{r}_2}\delta_{\mu,\nu}$ is satisfied. The Cooper pair charge is $Q=2e$, and E_{J_1} and E_{J_2} are the Josephson coupling constants within each array. $\tilde{\mathbf{C}}^{-1}_{\mu,\nu}$ is the electric field propagator and its inverse, $\mathbf{C}_{\mu,\nu}$, is the block geometric capacitance matrix. The frustration link variables $f(\vec{r}_1,\vec{r}_2)$ are defined by the line integral along the path that joins sites located at $\vec{r}_1$ and $\vec{r}_1$, that is, $f(\vec{r}_1,\vec{r}_2)=(1/\Phi_0)\int_{\vec{r}_2}^{\vec{r}_1}\vec{A}\cdot d\vec{l}$, with $\vec{A}$ as the magnetic vector potential and Φ_0 as the magnetic flux quantum. These variables are defined on the lattice bonds. The frustration index f is defined as a sum over a plaquette, $f=\Sigma_{\mathcal{P}} f(\vec{r}_1,\vec{r}_2)$. Here, we will consider two uniformly frustrated cases, $f=1/2$ and $f=1/3$. This means that on average, half of Φ_0—fully frustrated—or one-third of Φ_0 threads each elementary plaquette. In what follows, we will use the notation $\mathbf{C}_{\mu,\mu}=\mathbf{C}_\mu$ to denote the diagonal capacitance matrix. The block capacitance matrices were defined by Eqs. (2) and (3) in Paper I.[72]

To evaluate the partition function Ξ, we can calculate the trace over the phase operators $\hat{\phi}$ or over the trace of the number operators $\hat{\mathbf{n}}$. The path integral representation of Ξ can be derived using the coherent state representation[77]

$$\langle n(\vec{r}_1)|\phi(\vec{r}_2)\rangle = \frac{\exp[in(\vec{r}_1)\phi(\vec{r}_2)]}{\sqrt{2\pi}}\delta_{\vec{r}_1,\vec{r}_2}. \quad (2)$$

Following the steps outlined in Ref. 23, we obtain the lattice path integral representation of the partition function studied in this paper,

$$\Xi = \prod_{\tau=0}^{L_\tau-1}\prod_{\vec{r}}\sum_{n(\tau,\vec{r})}\int_0^{2\pi}\frac{d\phi(\tau,\vec{r})}{2\pi} \times\exp\left[-\int_0^{\beta\hbar}d\tau\left(\sum_{\vec{r}_1,\vec{r}_2}\frac{Q^2}{2}n(\tau,\vec{r}_1)\mathbf{C}^{-1}(\vec{r}_1,\vec{r}_2)n(\tau,\vec{r}_2) + i\sum_{\vec{r}}n(\tau,\vec{r})\frac{d\phi}{d\tau}(\tau,\vec{r}) + E_J\sum_{\langle \vec{r}_1,\vec{r}_2\rangle}\{1-\cos[\phi(\tau,\vec{r}_1) - \phi(\tau,\vec{r}_2)-2\pi f(\vec{r}_1,\vec{r}_2)]\}\right)\right]. \quad (3)$$

Here, the statistical variables are the scalar phases $\phi(\tau,\vec{r})$ and the scalar charge integer fields $\hat{n}(\tau,\vec{r})$ defined in a three-dimensional lattice, with two spatial dimensions L_x and L_y and the imaginary time L_τ axis. The angular phases, $\phi(\tau,\vec{r})\in[0,2\pi]$, are defined at the nodes of the lattice with periodic boundary conditions in the x and y space dimensions. The integer fields $\hat{n}(\tau,\vec{r})$ lie on the bonds between two consecutive sites along the imaginary time axis τ, and they can take any positive and negative integer values. The quantization condition in Ξ is defined in terms of the imaginary time periodic boundary conditions $\phi(L_\tau,\vec{r})=\phi(0,\vec{r})$. The $L_\tau\to\infty$ limit has been formally taken to replace the sum over imaginary time slices by its integral. This Ξ representation is amenable to numerical computations in contrast to evaluating its operator representation.

The arrays can be in a superconducting, insulating, or normal states depending on the values of T, α, and $C_{\rm int}$. To characterize the superconducting or the normal state behaviors, we calculated the helicity modulus Υ for each array defined by the derivatives of the free energy $\mathcal{F}$,

$$\Upsilon = \left.\frac{\partial^2\mathcal{F}}{\partial k^2}\right|_{k=0}. \quad (4)$$

Υ measures the energy needed to carry out a phase twist between the boundaries of the array along the $\vec{k}$ direction. The helicity modulus is proportional to the superfluid density per unit mass ρ_s,

$$\rho_s(T) = \frac{1}{V}\left(\frac{ma}{\hbar}\right)\Upsilon(T). \quad (5)$$

Here, a is the lattice spacing, m the Cooper pair mass, and V the volume. Combining Eqs. (3) and (4), we obtain the path

integral representation of the helicity modulus when the twist is along the $\vec{x}$ axis,[23]

$$\frac{1}{E_{J_\nu}L_xL_y}\Upsilon_\nu^x(T)=\frac{1}{L_xL_yL_\tau}\Bigg[\Bigg\langle\sum_{\tau=0}^{L_\tau-1}\sum_{\vec{r}_\nu}\cos[\phi(\tau,\vec{r}_\nu)-\phi(\tau,\vec{r}_\nu+\hat{x})-2\pi f(\vec{r}_\nu,\vec{r}_\nu+\hat{x})]\Bigg\rangle-\frac{E_{J_\nu}\beta}{L_\tau}\frac{E_{J_\nu}\beta}{L_\tau}\Bigg\{\Bigg\langle\Bigg\{\sum_{\tau=0}^{L_\tau-1}\sum_{\vec{r}_\nu}\sin[\phi(\tau,\vec{r}_\nu)-\phi(\tau,\vec{r}_\nu+\hat{x})-2\pi f(\vec{r}_\nu,\vec{r}_\nu+\hat{x})]\Bigg\}^2\Bigg\rangle-\Bigg\langle\sum_{\tau=0}^{L_\tau-1}\sum_{\vec{r}_\nu}\sin[\phi(\tau,\vec{r}_\nu)-\phi(\tau,\vec{r}_\nu+\hat{x})-2\pi f(\vec{r}_\nu,\vec{r}_\nu+\hat{x})]\Bigg\rangle^2\Bigg\}\Bigg]. \tag{6}$$

The array charge coherence is determined by the inverse dielectric constant ϵ^{-1} defined as

$$\epsilon^{-1}=\lim_{\vec{q}\to 0}\left[1-\frac{Q^2}{k_BT}\frac{1}{\mathbf{C}(\vec{q})}\langle n(\vec{q})n(-\vec{q})\rangle\right]. \tag{7}$$

Combining Eqs. (3) and (7), as well as Fourier transforming the capacitance matrix and the charge number operator,[23] we can write the path integral representation of the charge number correlation function $\langle n(\vec{r}_1)n(\vec{r}_2)\rangle$ as

$$\langle n(\vec{r}_1)n(\vec{r}_2)\rangle=\frac{1}{\beta Q^2}\mathbf{C}(\vec{r}_1,\vec{r}_2)+\left(\frac{2\pi}{\beta L_\tau}\right)^2\sum_{\vec{r}_3,\vec{r}_4}\mathbf{C}(\vec{r}_1,\vec{r}_3)\mathbf{C}(\vec{r}_2,\vec{r}_4)\times\langle m(\vec{r}_3),m(\vec{r}_4)\rangle. \tag{8}$$

The integer fields $m(\vec{r})$'s represent the charge degrees of freedom of the system. Substituting this result in Eq. (7) yields the inverse dielectric constant expression

$$\epsilon^{-1}=\lim_{\vec{k}\to 0}\left[\frac{(2\pi)^2}{\beta Q^2}\mathbf{C}(\vec{k})\langle|m(\vec{k})|^2\rangle\right]. \tag{9}$$

In these equations, the path integral representation of the integer fields $m(\vec{r})$'s is $m(\vec{r})=\Sigma_{\tau=0}^{L_\tau-1}m(\tau,\vec{r})$. It is important to note that the path integral representation of ϵ^{-1} in Eq. (9) is not exactly the inverse dielectric function of a gas of Cooper pairs since it depends on the discretization of the imaginary time axis in L_τ slices. Nonetheless, we expect that it contains most of the relevant information of the dielectric properties of the gas of Cooper pairs in the arrays.

III. RESULTS AND DISCUSSION

A. Description and parameters of the simulations

To carry out the quantum MC updates in the phases, we used the standard Metropolis algorithm. To speed up the calculations, we replace the $U(1)$ continuous symmetry in the phases by a discrete $\mathbf{Z}_N$ subgroup.[7] Using $N=5000$ proved to yield accurate results. Discretizing the phases has the advantage of using integer arithmetic that allows us to build cosine tables for the Boltzmann factors in the partition function. This simplification cannot be used for the integer fields, except when $C_m=0$. In that case, the $m(\tau,\vec{r})$ fields can be summed up exactly. This approach allows us to build up look up tables that introduce an adequate effective potential.[23]

Once the system reaches thermal equilibrium after N_{ther} (between 10^3 and 10^4) MC sweeps, the thermodynamic averages were calculated. A measure was taken after N_{sweeps} passes through the arrays updating the phases, and M_{sweeps} passes updating the integer fields. In the semiclassical limit, $\alpha\ll 1$, it was sufficient to consider $N_{sweeps}=4$ and $M_{sweeps}=4$ at high temperatures ($T>0.25$), and $N_{sweeps}=10$ and $M_{sweeps}=10$ at low temperatures ($T<0.25$). In the quantum limit, $\alpha>1$, we took $N_{sweeps}=4$ and $M_{sweeps}=4$ at high temperatures, and $N_{sweeps}=10$ and $M_{sweeps}=10$ at low temperatures. These parameter values were chosen to minimize the decorrelation times due to the long-range charge interactions. Proceeding in this way, we carried out averages over 16 384 MC steps at high temperatures and 32 768 at low temperatures. Error bars were calculated using the biased reduction method described in Ref. 78.

For each frustration f value, we studied the helicity modulus and the inverse dielectric constant for each array as a function of temperature, α, and the ratio of the interlayer self-capacitance to the intralayer mutual capacitance C_{int}. The normalized temperature, $T^*=(k_BT)/E_J$, that from now on will be denoted simply by T was varied in the range $[0.02,0.5]$ in 0.05 steps at high T's and 0.02 steps at low T's. To study the transition between the semiclassical and quantum states, the quantum parameter in one array was kept fixed at $\alpha_1=0.5$, while we varied α_2 of the second array taking the values $\alpha_2=0.5$, 1.0, 1.25, 1.50, 2.0, 2.5, 3.0, and 4.0. In addition, the capacitance ratios were integer multiples of the Delft's experimental parameters:[39] $C_{\text{int}}=\kappa\times 0.260\,87$, with $\kappa=1$, 2, 3, 4, and 5. The values chosen for this ratio allowed us to study the capacitive coupling effects between the arrays, going from weak to the strong coupling regime when $\kappa\geqslant 3$. The spatial lattice was determined by the $f=p/q$ value since the lattice size must be a multiple of the ground state elementary plaquette size, $p\times q$. According to this the simulations were carried out for lattice sizes $L_x\times L_y=32\times 32$ for $f=1/2$ and $L_x\times L_y=36\times 36$ for $f=1/3$. In both cases, the length of the imaginary time axis was $L_\tau=96$ for $0.5\leqslant\alpha\leqslant 2.0$ and L_τ up to 128 for higher values $2.0<\alpha\leqslant 4.0$. The larger the value of α, the larger the length of the imaginary time axis. For the L_τ values chosen, we obtained reliable accurate results, with negligible finite size effects along the imaginary time axis.

B. Results for Υ and ϵ^{-1} at full frustration, $f=1/2$

In this subsection, we present and discuss our results for $\Upsilon_{1,2}(T,\alpha_2)$ and $\varepsilon_{1,2}^{-1}(T,\alpha_2)$ at full frustration, $f=1/2$. The study was carried out for different parameter values of α_2, keeping $\alpha_1=0.5$ fixed, and for different values of the cou-

pling capacitance between the arrays. We start by discussing the case when both arrays are in the semiclassical regime but with different values of α_i, that is, $\alpha_1=0.5$ and $\alpha_2=1.0$ with $0.260\,87 \leqslant C_{\rm int} \leqslant 1.304\,35$. We briefly describe the corresponding results to compare, where appropriate, with previous studies and with other parameter values considered here. We found that there is a low-temperature regime that depends on the value of α_i, where $\Upsilon_{1,2}$ are nonzero—SC phases—with $\Upsilon_1(T,\alpha_1=0.5) > \Upsilon_2(T,\alpha_2=1.0)$ and with relatively small fluctuations around their average values. As temperature increases, both quantities decrease monotonically down to zero at the transition temperatures $T_{\rm sc}(\alpha_{1,2})$, with $T_{\rm sc}(\alpha_1) > T_{\rm sc}(\alpha_2)$. For $T \geqslant T_{\rm sc}(\alpha_{1,2})$, they were equal to zero, indicating that at high temperatures, the arrays were in the normal state. About the transition temperatures $T_{\rm sc}(\alpha_{1,2})$, the $\Upsilon_{1,2}$ fluctuations became larger as expected. Since both arrays were in the semiclassical regime, the charges did not play any role in the system dynamics, except for a small decrease in phase coherence, that led to a lower transition temperature, and we obtained $\epsilon_{1,2}^{-1}=0$ for $T>0$. We also found that the capacitive couplings considered here did not change the nature of the transitions nor the $T_{\rm sc}(\alpha_{1,2})$ values. These semiclassical array results are in agreement with previous studies for one array,[7–9,23] and for two capacitively coupled JJAs in zero magnetic field.[72] The results described here indicate that when both arrays were in the semiclassical regime, the transition temperatures $T_{\rm sc}(\alpha)$ were not affected by the interlayer capacitive coupling and charges did not play any significant role in the array behavior.

As the quantum parameter of array 2 increased to $\alpha_2=1.25$, the of $\epsilon_{1,2}^{-1}(T,\alpha_{1,2})$ and $\Upsilon_{1,2}(T,\alpha_{1,2})$ behaviors showed that charge coherence starts to develop in array 2 at very low temperatures, for the five capacitive coupling values ($\kappa=1,2,3,4,5$) considered here. At the same time and as one would expect, we observed a slight decrease in the second array phase coherence at low temperatures, but we do not see any significant change in the phase coherence of array 1.

A further increase in the charging energy of array 2, to $\alpha_2=1.5$, leads to its complete loss of phase coherence at low temperatures. As seen in the top panels of Fig. 1, $\Upsilon_2(T,\alpha_2)$ (▼) decreases down to zero for $T \leqslant 0.06$ and for $C_{\rm int}=0.260\,87$ and $0.521\,74$. That is, there is a reentrant SC-N phase transition in the quantum array. Nonetheless, for higher values of the capacitive coupling between arrays, $C_{\rm int}$, $1.043\,48$ and $1.304\,35$, this reentrance in the phase degrees of freedom disappears. Instead, one observes a decrease of the helicity modulus at relatively low temperatures and then a slight increase at lower temperatures. We also note at the bottom panels of Fig. 1 that for the capacitive coupling values, $C_{\rm int}=0.260\,87$ and $0.521\,74$, in the low-temperature range where $\Upsilon_2(T,\alpha_2)$ goes down to zero, $\epsilon_2^{-1}(T,\alpha_2)$ increases significantly as a signature of the existence of charge coherence that leads to an insulating phase. However, as the capacitive coupling between the arrays increases, $C_{\rm int}=1.043\,48$ and $1.304\,35$, there is a significant decrease in $\epsilon_2^{-1}(T,\alpha_2)$, that is, charge coherence diminishes.

Thus, as temperature decreases, array 2 undergoes a N-SC transition at intermediate temperatures and a SC-I phase transition at lower temperatures, with the behavior of the semi-

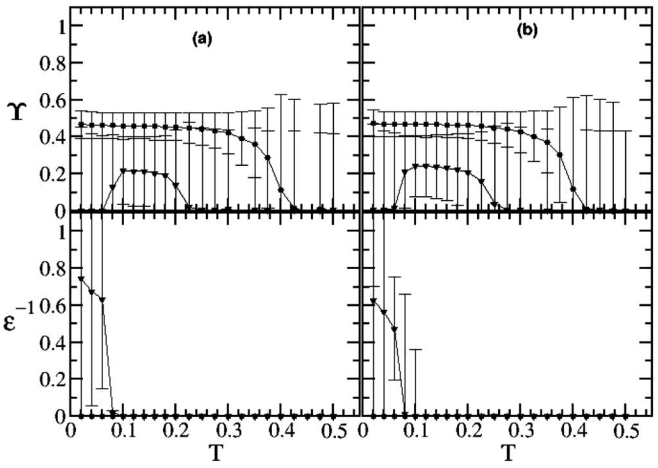

FIG. 1. Υ and ϵ^{-1} as a function of temperature at full frustration, $f=1/2$. The values for the α_i quantum parameters are $\alpha_1=0.5$ (●), for the semiclassical array, and $\alpha_2=1.5$ (▼), for the quantum array. The capacitive couplings between the arrays, $C_{\rm int}$, are (a) 0.260 87 and (b) 0.521 74.

classical array (array 1) not affected. That is, it develops phase coherence for $T \leqslant 0.4$, as an indication of the existence of a N-SC transition. In Fig. 2, we show, for the same values of α_1 and α_2 but for larger capacitive couplings $C_{\rm int}=0.782\,61$ and $1.043\,48$, that for $T \leqslant 0.06$, phase coherence appears to increase, while charge coherence appears to decrease in the quantum array (array 2). Similar behavior, although not shown explicitly here, was obtained for $C_{\rm int}=1.304\,35$. These decrease and increase at low temperatures in $\Upsilon_2(T)$ are similar to the one found at zero magnetic field.[72] This is consistent with the dual behavior between vortices and charges due to their *gauge capacitive interaction*, as predicted in Ref. 71. As a consequence, the fluctuations in the helicity modulus and the inverse dielectric constant are much stronger than those observed in the semiclassical limit in a single array, and the quantum fluctuations in the second array are not sufficiently strong to significantly affect the first array

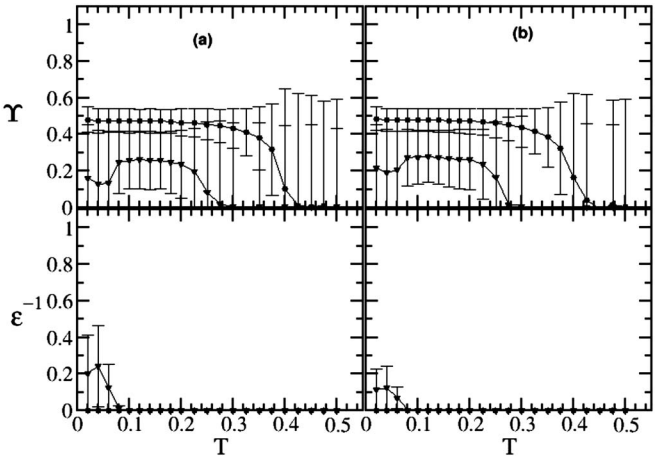

FIG. 2. Υ and ϵ^{-1} as a function of temperature at $f=1/2$, full frustration. The values for the quantum parameters are $\alpha_1=0.5$ (●) and $\alpha_2=1.5$ (▼). The capacitive couplings between the arrays, $C_{\rm int}$, are (a) 0.782 61 and (b) 1.043 48.

semiclassical behavior. This means that the gauge interaction between vortex and charge Coulomb gases is weak. As array 2 goes further into the quantum regime, $\alpha_2=1.75$, we found that for the lowest capacitive coupling considered here, $C_{\rm int}=0.260\,87$, $\Upsilon_2(T)\approx 0$ at all temperatures, indicating a complete absence of phase coherence in array 2. However, we found that at $T\approx 0.08$, $\epsilon_2^{-1}(T)$ jumped from zero up to $\epsilon_2^{-1}(T)\approx 0.80$ for $T<0.08$ as an indication that charge coherence has fully developed, again due to the duality between vortices and charges. Further increasing the capacitive coupling between the arrays to $C_{\rm int}=0.521\,74$, $0.782\,61$, $1.043\,48$, and $1.304\,35$ yields a nonzero helicity modulus for the quantum array at intermediate temperatures and its decrease down to zero at lower temperatures. In this temperature regime, $\epsilon_2^{-1}(T)$ is nonzero. These results indicate again the existence of N-SC-I transitions in the quantum array, while in the semiclassical array, $\Upsilon_1(T)>0$ for $T\leqslant 0.42$ and $\epsilon_1^{-1}(T)=0$ at all temperatures. The N-SC-N reentrant transition found as a function of the capacitive coupling is a novel phenomenon that allows one to tune the phase coherent behavior of array 2 by varying the coupling between the arrays. It is clearer as array 2 goes further into the quantum regime, as will be discussed below. We do not include the corresponding figure explicitly showing this behavior since it is similar to that shown in Fig. 2. Increasing even more the quantum parameter of array 2 to $\alpha_2=2.0$ while keeping array 1 in the semiclassical regime, $\alpha_1=0.5$, leads to a different scenario as function of the capacitive coupling. We found that array 1 shows SC behavior for $T<T_{\rm sc}(\alpha)$ for all considered values of $C_{\rm int}$. Nonetheless, for $C_{\rm int}=0.260\,87$ and $0.521\,74$, no phase coherence occurs in array 2. For higher values of the capacitive coupling, $C_{\rm int}=0.782\,61$, $1.043\,48$, and $1.303\,48$, we found that phase coherence develops gradually in array 2 for intermediate temperatures and goes down to zero at lower and higher temperatures. Again, increasing the capacitive coupling appears to induce a N-SC-N reentrant phase transition in array 2 at intermediate temperatures. In addition, we found $\epsilon^{-1}(T,C_{\rm int})>0$ at low temperatures for all values of $C_{\rm int}$ considered in the simulations. This indicates the existence of a N-I transition. In Fig. 3, we show $\Upsilon_{1,2}(T)$ and $\epsilon_{1,2}^{-1}(T)$, explicitly showing the phase coherent behavior described above.

When array 2 is such that $2.0<\alpha_2\leqslant 4$ and array 1 is at $\alpha_1=0.5$, it is found that the former shows no evidence of a superconducting phase, while the latter develops phase coherence. However, when we looked at the charge degrees of freedom, it was found that array 2 developed charge coherence at low temperatures for all the values of $C_{\rm int}$, while array 1 showed no evidence of an insulating phase, that is, $\epsilon^{-1}(T,C_{\rm int})=0$ at all T's considered here.

C. Results for Υ and ϵ^{-1} at frustration, $f=1/3$

In this subsection, we present and discuss the $\Upsilon_{1,2}(T,\alpha_2)$ and $\varepsilon_{1,2}^{-1}(T,\alpha_2)$ results for $f=1/3$. We analyzed the behavior of these quantities for $\alpha_1=0.5$ fixed, different values of the quantum parameter α_2, as functions of temperature and capacitive coupling. As in the full frustration case, we started considering the situation when both arrays were in the semiclassical regime, that is, $\alpha_1=0.5$ and $\alpha_2=1.0$. Unlike the fully frustrated case, we found that $\Upsilon_{1,2}(T,\alpha_{1,2})=0$ at all temperatures and capacitive coupling values $0.260\,87\leqslant C_{\rm int}\leqslant 1.304\,35$. Thus, no phase coherence was established in any of the two coupled arrays. However, we found that array 2 developed charge coherence for $T\leqslant 0.1$, that is, $\epsilon_2^{-1}(T)>0$, for all capacitive couplings considered. In contrast, it was found that $\epsilon_1^{-1}(T,\alpha_1)=0$ at all temperatures. However, $\epsilon_2^{-1}(T)$ decreased as the interlayer capacitive coupling increased, as shown in Fig. 4. Further increasing the quantum parameter of array 2 to $\alpha_2=1.5$ and 1.75 while keeping $\alpha_1=0.5$ and $0.260\,87\leqslant C_{\rm int}\leqslant 1.304\,35$ yielded similar results for both $\Upsilon_{1,2}(T,\alpha)$ and $\epsilon_{1,2}^{-1}(T,\alpha)$, as those described in the previous paragraph.

A further increase to $\alpha_2=2.0$, with $\alpha_1=0.5$, led to a different phase behavior in array 1. We found $\Upsilon_1(T,\alpha_2)>0$ in the temperature range $0<T_1<T<T_2$, and zero otherwise.

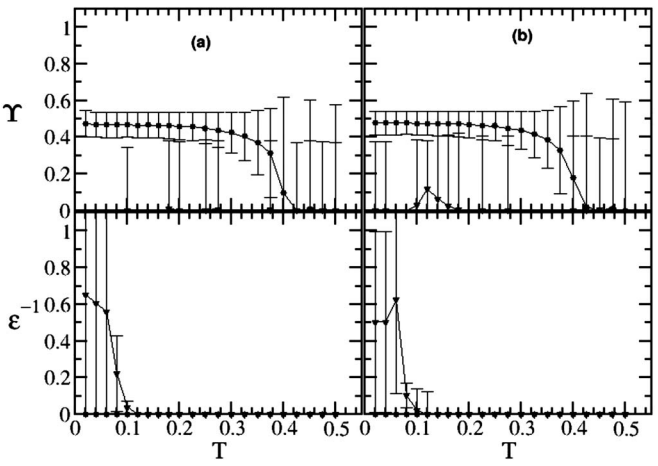

FIG. 3. Υ and ϵ^{-1} as a function of temperature at $f=1/2$, full frustration. The values for the quantum parameters are $\alpha_1=0.5$ (●) and $\alpha_2=2.0$ (▼). The capacitive couplings between the arrays, $C_{\rm int}$, are (a) 0.521 74 and (b) 1.043 48.

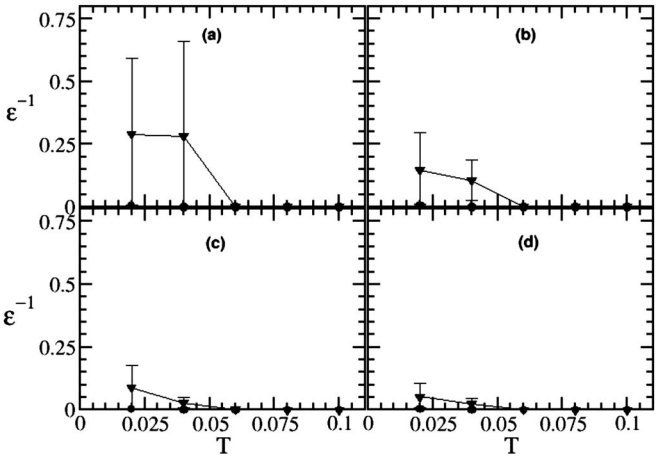

FIG. 4. Inverse dielectric constant behavior for $\alpha_1=0.5$ (●) and $\alpha_2=1.0$ (▼) for frustration $f=1/3$. Each plot corresponds to a capacitive coupling, $C_{\rm int}$=(a) 0.521 74, (b) 0.782 61, (c) 1.043 48, and (d) 1.304 35. Note that ϵ^{-1} decreases as the capacitive coupling increases.

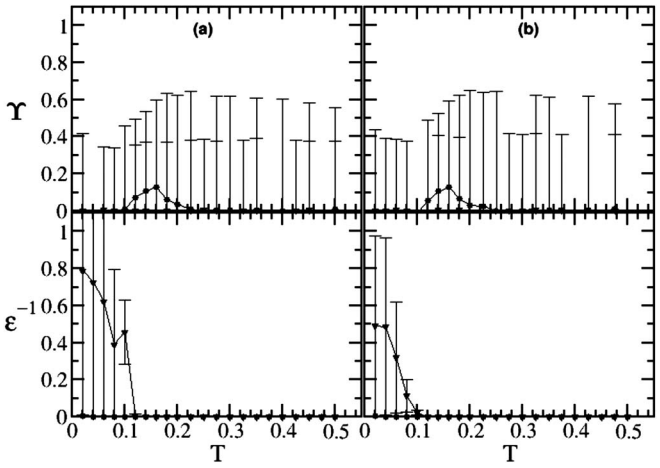

FIG. 5. Υ and ϵ^{-1} as a function of temperature at frustration, $f=1/3$. Here, $\alpha_1=0.5$ (●) and $\alpha_2=2.0$ (▼). The capacitive couplings between the arrays, C_{int}, are (a) 0.260 87 and (b) 1.043 48.

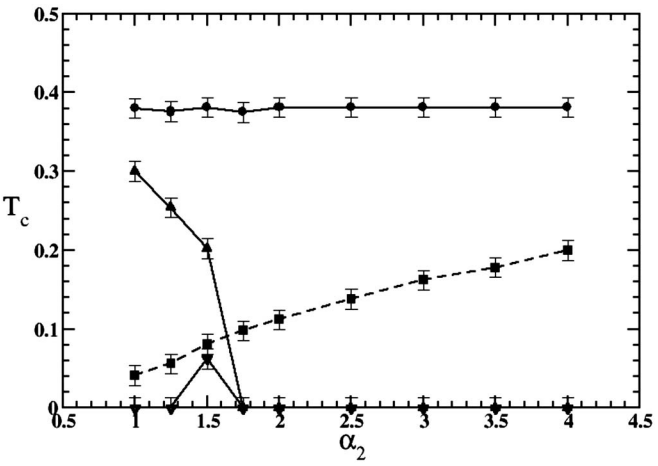

FIG. 6. Estimated transition temperatures for each array vs α_2 for frustration $f=1/2$ and $C_{\text{int}}=0.260\,87$. SC-N phase boundary for the semiclassical array 1 (●). Notice that array 2 develops two SC-N boundaries: a regular one (▲) and a reentrance line (▼). The solid lines represent the SC-N phase boundary, while the dashed line the I-N phase boundary (■). The lines are a guide to the eyes and do not represent the result of a fitting or an interpolating procedure.

This result suggests the existence of a new reentrant N-SC-N transition in the semiclassical array. This is surprising since this kind of behavior had not been previously found neither in the unfrustrated nor for the fully frustrated capacitively coupled JJAs. This behavior should be related to the underlying $f=1/3$ ground state symmetries. On the other hand, it was found that the quantum array 2 showed no phase coherence, that is, $\Upsilon_2(T,\alpha_2)=0$, for all temperatures and capacitive couplings considered here. For the charge degrees of freedom, it was found that $\varepsilon_1^{-1}(T)=0$ at all temperatures, while $\varepsilon_2^{-1}(T)>0$ at temperatures $T<T_1$, but close to T_1. Here, T_1 is the lowest temperature at which $\Upsilon_1(T,\alpha_2)$ drops to zero. This behavior in both degrees of freedom holds for all capacitive coupling values between arrays 1 and 2 considered here. Figure 5 shows the behavior just described for $\Upsilon_{1,2}(T,\alpha_2)$ as well as for $\varepsilon_{1,2}^{-1}(T)$ for $\alpha_1=0.5$ and $\alpha_2=2.0$. Thus, there appears to be a phase coherence onset in the semiclassical array before the quantum array develops charge coherence at low temperatures. Again, this is a manifestation of the charge and vortex—thermal plus magnetic vortices—duality.

D. Phase diagrams

In this subsection, we present the phase diagrams that were obtained from the critical temperature estimations from $\Upsilon_{1,2}(T,\alpha_2)$ and $\epsilon_{1,2}^{-1}(T,\alpha_2)$ for different values of the coupling capacitance between arrays and for magnetic frustration values $f=1/2$ and $f=1/3$.

The quantum parameter of array 1, $\alpha_1=0.5$, was kept fixed, while the quantum parameter of array 2, α_2, was varied in the interval $1.0\leqslant\alpha_2\leqslant4.0$, in $\Delta\alpha_2=0.25$ steps, for each one of the values of C_{int} and $f=1/2$ and $1/3$. The transition temperatures were estimated from the behavior of $\Upsilon_{1,2}(T,\alpha_2)$ and $\varepsilon_{1,2}^{-1}(T,\alpha_2)$ as a function of temperature. According to the Berezinskii-Kosterlitz-Thouless (BKT) criteria, for a classical array, the critical SC-N temperature occurs at the intercept of the helicity modulus with a straight line with slope $2/\pi$. In the quantum arrays, it has been shown experimentally that in the limit $C_s/C_m\to0$, there is a crossover from a conducting to an insulating phase.[38,40,45] Due to the finite size of the arrays, there is a rounding of the transitions because the screening length is shorter than the size of the arrays.[39] Theoretically, it has been argued that for any finite screening length, the phase transition is washed out even in classical arrays of infinite size.[79] This happens because the BKT SC-N scenario crucially depends on the unscreened nature of the logarithmic interaction between vortex pairs.[76,80] Nonetheless, it has been recently shown[29,30] that even in the regime of strong quantum fluctuations, the data for $\Upsilon(T)$ at low temperatures can be very well fitted to the Kosterlitz's renormalization group equations in a finite size Υ analysis. Here, we will still use the BKT fitting theory since we have not carried out a detailed finite size analysis due to the fact that even the calculations done here were computationally very extensive and demanding. When there is a low-temperature reentrant transition, the transition temperature is determined from the temperature at which $\Upsilon_{1,2}(T,\alpha_2)$ or $\varepsilon_{1,2}^{-1}(T,\alpha_2)$ vanish as it is done with the arrays's electric resistance in experiments.[47] The error bars in the transition temperatures were estimated in the calculations by taking into account the size of the temperature variation step, δT. Since $\delta T=0.05$, the error bars in the transition temperatures of the phase boundaries are $\delta T_c=0.05$.

In Fig. 6 we show the phase diagrams for T_c versus α_2 for the phase and charge degrees of freedom for arrays 1 and 2, when $C_{\text{int}}=0.260\,87$ and $f=1/2$. We show that the SC-N phase boundary (●) of the semiclassical array 1 remains almost unchanged as a function of α_2, with $T_c\simeq0.45$. The SC-N phase boundary of array 2, however, changes significantly as α_2 increases. The transition temperature decreases linearly for $1.0\leqslant\alpha_2\leqslant1.75$, reaching zero at $\alpha_2=1.75$. One also sees that when $1.25\leqslant\alpha_2\leqslant1.75$, there is a reentrant N-SC-N transition in array 2. The points that delimit this

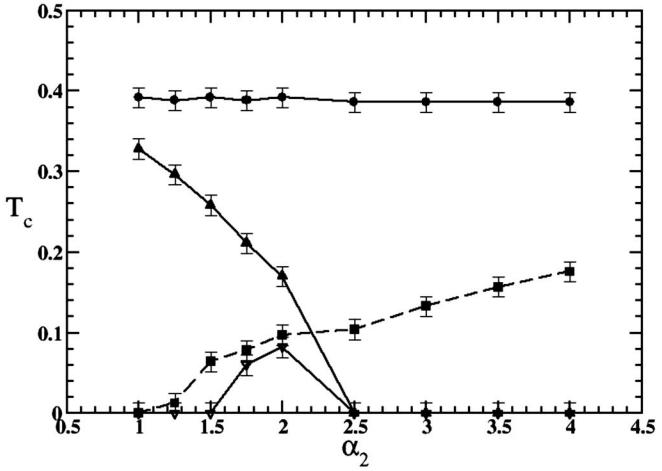

FIG. 7. Same as in Fig. 6 but with an interlayer capacitive coupling $C_{\text{int}}=1.043\ 48$.

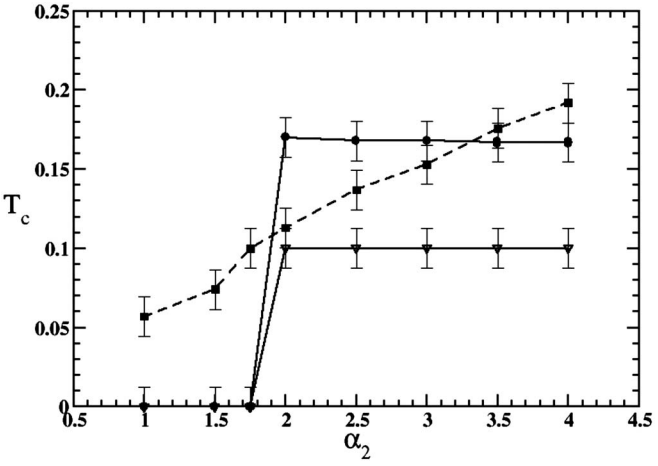

FIG. 8. Estimated transition temperatures of each array vs α_2 for frustration $f=1/3$ and $C_{\text{int}}=0.521\ 74$. Note that array 1 develops a regular SC-N boundary (●) and a reentrance SC-N line (▼). Nonetheless, array 2 does not show a SC-N boundary at all. The solid lines represent the SC-N phase boundary, while the dashed lines the I-N phase boundary. The lines are a guide to the eyes and do not represent the result of a fitting or an interpolating procedure.

boundary have been denoted by (▼). The I-N phase boundary (■) increases monotonically as α_2 increases. As the capacitive coupling between these arrays increases, the features of the phase diagrams remain essentially the same except for the fact that at $\alpha_2=1.0$ and for $C_{\text{int}}\geqslant 0.782\ 61$, the transition temperature drops to zero. In Fig. 7, we show the corresponding phase diagram for $C_{\text{int}}=1.303\ 45$.

We now turn to the phase diagram description when $f=1/3$. In this case, we found that the semiclassical array shows a nonzero SC-N transition temperature for $\alpha_2\geqslant 2.0$ for all values of the capacitive coupling considered, while the quantum array shows no phase coherence at all. In addition, one sees that the transition temperature of array 1 remains almost constant as a function of α_2. For these values of the quantum parameter, we also found that there is a reentrant SC-N transition at lower temperatures. In this case, T_c remained constant. This boundary is indicated (▼) in Fig. 8. There, we have plotted the phase diagram T_c versus α_2 for $C_{\text{int}}=0.521\ 74$. The same figure shows that the I-N transition temperature (■) increases monotonically as a function of α_2. As the coupling between the arrays increases, we found that the features of the corresponding phase boundaries follow essentially the same trend described in the previous paragraph for $C_{\text{int}}=0.521\ 74$. For the sake of completeness, in Fig. 9, we show the phase diagram results for $C_{\text{int}}=1.303\ 45$ that, as already mentioned, is similar to the other values for the capacitive coupling.

IV. CONCLUSIONS

We have carried out extensive path integral quantum MC simulations of two capacitively coupled and uniformly frustrated JJAs made of ultrasmall Josephson junctions. One of the arrays is maintained in the semiclassical regime ($\alpha_1=0.5$), while the other was in the semiclassical or in the extreme quantum regimes. Here, we did not explicitly study the excitation dynamics of the Z_2 and $Z_2\times Z_3$ symmetries associated with frustrations $f=1/2$ and $f=1/3$, respectively. A detailed analysis of these degrees of freedom would have required a huge amount a CPU time since they need to be monitored and calculated for each array at each one of the time slices along the imaginary time axis. A corresponding calculation and analysis will be carried out in a future communication. Instead, in this paper, we focused on deriving the phase diagrams due to the phase and charge degrees of freedom. We studied the helicity modulus and the inverse dielectric constant of each array as a function of temperature and quantum parameter α_2, for different values of the interlayer capacitances and frustration parameter. When the array phases are at full frustration ($f=1/2$) and both arrays are in the semiclassical regime $\alpha_{1,2}<1.5$, regardless of the interlayer coupling considered here, each array, shows a SC-N transition at finite temperatures. For these semiclassical arrays, the charge degrees of freedom contribution is negligible and there is no I-N transition at finite temperatures. As array 2 enters the quantum regime ($\alpha_2=1.5$ and 1.75), a SC-N

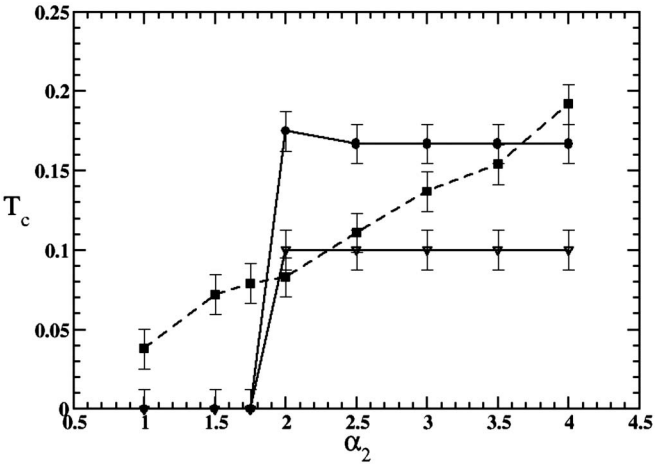

FIG. 9. Same as in Fig. 8 with $C_{\text{int}}=1.303\ 45$.

reentrant phase transition develops in this array at intermediate temperatures, while at lower temperatures, there is an I-N transition. We also found that the fluctuations in Υ_2 and ϵ_2^{-1} became significantly larger due to quantum fluctuations, as explained in Ref. 29. This scenario occurred for all the values of the interlayer capacitive coupling considered here. Dissipation was not considered here but it is known that for large enough dissipation, the quantum fluctuations are quenched.[31,32] Dissipation can, in fact, suppress the zero-temperature quantum phase transition, as well as the reentrant behavior found for a single quantum JJA.[29]

At the particular value $\alpha_2=2.0$, we found that for low capacitive couplings between the arrays, $C_{\text{int}}=0.260\,87$ and 0.521 74, no phase coherence occurs in array 2. Nonetheless, as the coupling goes from $C_{\text{int}}=0.782\,61$ to higher values, 1.043 48 and 1.304 35, array 2 starts to develop a N-SC-N reentrant transition at intermediate temperatures. Thus, the capacitive coupling induces this novel reentrant transition. In addition, we found a N-I transition in array 2 at lower temperatures. For higher values of $\alpha_2>2.0$, no phase transition (SC-N) occurs in array 2. Nevertheless, we do find an I-N transition at lower temperatures.

Unlike the fully frustrated case, when the arrays are at frustration $f=1/3$, we found that for $1.0\leqslant\alpha_2<2.0$, no SC-N transition is present in both arrays. However, array 2 develops charge coherence at low temperatures and this coherence decreases slightly as the capacitive coupling increases. On the other hand, for $\alpha_2\geqslant 2$, array 1 undergoes a N-SC-N transition at intermediate temperatures, while array 2 does no show phase coherence. Since array 2 is in the quantum regime, it certainly develops charge coherence at low temperatures. This scenario happens for all values of the capacitive coupling considered in this paper. The results presented here can be tested experimentally in a system of the type developed in Ref. 41.

ACKNOWLEDGMENTS

G.R.-S. would like to acknowledge partial financial support from CONACYT-MEXICO through Contract No 43596-F and from DAGAPA-UNAM Contract No. IN110103. J.V.J thanks NSF for partial financial support.

[1] Editor's Business Note, Nature (London) **446**, 245 (2007).
[2] E. Simánek, Solid State Commun. **31**, 419 (1979); Phys. Rev. B **22**, 459 (1980); **23**, 5762 (1981).
[3] K. B. Efetov, Zh. Eksp. Teor. Fiz. **78**, 2017 (1980) [Sov. Phys. JETP **51**, 1015 (1980)].
[4] P. Fazekas, Z. Phys. B: Condens. Matter **45**, 215 (1982).
[5] P. Fazekas, B. Muhlschlegel and M. Schroter, Z. Phys. B: Condens. Matter **57**, 193 (1984).
[6] J. V. José, Phys. Rev. B **29**, 2836 (1984).
[7] L. Jacobs, J. V. José, and M. A. Novotny, Phys. Rev. Lett. **53**, 2177 (1984).
[8] L. Jacobs, J. V. José, M. A. Novotny, and A. M. Goldman, Europhys. Lett. **3**, 1295 (1987).
[9] L. Jacobs, J. V. José, M. A. Novotny, and A. M. Goldman, Phys. Rev. B **38**, 4562 (1988).
[10] S. Kim and M. Y. Choi, Phys. Rev. B **41**, 111 (1990).
[11] R. Fazio and G. Schön, Phys. Rev. B **43**, 5307 (1991).
[12] M. V. Simkin, Phys. Rev. B **44**, 7074 (1991).
[13] D. Ariosa and H. Beck, Phys. Rev. B **45**, 819 (1992).
[14] E. Granato and M. A. Contentino, Europhys. Lett. **18**, 343 (1992).
[15] J. G. Kissner and U. Eckern, Z. Phys. B: Condens. Matter **91**, 115 (1993).
[16] E. Granato and M. A. Continentino, Phys. Rev. B **48**, 15977 (1993).
[17] E. Roddick and D. Stroud, Phys. Rev. B **48**, 16600 (1993).
[18] J. V. José and C. Rojas, Physica C **203**, 481 (1994).
[19] E. Simanek, *Inhomogeneous Superconductors* (Oxford University Press, New York, 1994).
[20] A. van Otterlo and K-H. Wagenblast, Phys. Rev. Lett. **72**, 3598 (1994).
[21] B. J. Kim and M. Y. Choi, Phys. Rev. B **52**, 3624 (1995).
[22] C. Rojas, Ph.D. thesis, Northeastern University, 1995.
[23] C. Rojas and J. V. José, Phys. Rev. B **54**, 12361 (1996).
[24] Beam Jun Kim, Gun Sung Jeon, M. S. Choi, and M. Y. Choi, Phys. Rev. B **58**, 14524 (1998).
[25] M. Lee, M.-S. Choi, and M. Y. Choi, Phys. Rev. B **60**, 10455 (1999).
[26] G. Grignani, A. Mattoni, P. Sodano, and A. Trombettoni, Phys. Rev. B **61**, 11676 (2000).
[27] T. K. Kópec and Jorge V. José, Phys. Rev. Lett. **84**, 749 (2000); Phys. Rev. B **60**, 7473 (1999); Phys. Rev. B **63**, 064504 (2001).
[28] T. K. Kópec and T. P. Polak, Phys. Rev. B **66**, 094517 (2002).
[29] L. Capriotti, A. Cuccoli, A. Fubini, V. Tognetti, and R. Vaia, Phys. Rev. Lett. **91**, 247004 (2003).
[30] Iulian Hetal, Thomas R. Lemberger, and Mohit Randeria, Nat. Phys. **3**, 700 (2007).
[31] J. Choi and J. V. José, Phys. Rev. Lett. **62**, 1904 (1989).
[32] L. Capriotti, A. Cuccoli, A. Fubini, V. Tognetti, and R. Vaia, Phys. Rev. Lett. **94**, 157001 (2005).
[33] T. P. Polak and T. K. Kópec, Phys. Rev. B **72**, 014509 (2005).
[34] M. C. Diamantini, P. Sodano, and C. A. Trugenberger, Phys. Rev. Lett. **75**, 3517 (1995).
[35] L. J. Geerligs, M. Peters, L. E. M. de Groot, A. Verbruggen, and J. E. Mooij, Phys. Rev. Lett. **63**, 326 (1989).
[36] Proceedings of the NATO Advanced Research Workshop on Coherence on Superconducting Networks, Delft, Netherlands, 1987, edited by J. E. Mooij and G. B. Schön [Physica B 152, 1 (1988)]; Proceedings of the Second CTP Workshop on Statistical Physics: KT Transition and Superconducting Arrays, edited by D. Kim, J. S. Chung, and M. Y. Choi (Min Eum Sa, Seoul, 1993).
[37] J. E. Mooij, B. J. van Wess, L. J. Geerlings, M. Peters, R. Fazio, and G. Schön, Phys. Rev. Lett. **65**, 645 (1990).
[38] H. S. J. van der Zant, Ph.D. thesis, Delft University, 1991.
[39] H. S. J. van der Zant, L. J. Geerlings, and J. E. Mooij, Europhys.

Lett. **19**, 541 (1992).
[40] T. S. Tighe, M. T. Tuominen, J. M. Hergenrother, and M. Tinkham, Phys. Rev. B **47**, 1145 (1993).
[41] R. Fazio and H. van der Zant, Phys. Rep. **355**, 235 (2001).
[42] L. L. Sohn, J. Romijn, E van der Drift, W. J. Elion, and J. E. Mooij, Physica B **194-196**, 125 (1994).
[43] Y. Takahide, R. Yagi, A. Kanda, Y. Ootuka, and S. I. Kobayashi, Phys. Rev. Lett. **85**, 1974 (2000).
[44] D. B. Haviland, K. Anderson, and P. Agren, J. Low Temp. Phys. **118**, 733 (2000).
[45] P. Delsing, C. D. Chen, D. B. Haviland, Y. Harada and T. Claeson, Phys. Rev. B **50**, 3959 (1994).
[46] W. J. Elion, Ph.D. thesis, Delft University, 1995.
[47] H. S. J. van der Zant, W. J. Elion, L. J. Geerligs, and J. E. Mooij, Phys. Rev. B **54**, 10081 (1996).
[48] A. Stern, Phys. Rev. B **50**, 10092 (1994).
[49] A. A. Odintsov and Y. Nazarov, Phys. Rev. B **51**, 1133 (1995); Physica B **203**, 513 (1994).
[50] M. Y. Choi, Phys. Rev. B **50**, 10088 (1994).
[51] S. Teitel and C. Jayaprakash, Phys. Rev. B **27**, 598 (1983).
[52] W. Y. Shih and D. Stroud, Phys. Rev. B **30**, 6774 (1984).
[53] G. S. Grest, Phys. Rev. B **39**, 9267 (1989).
[54] J. Lee, J. M. Kosterlitz, and E. Granato, Phys. Rev. B **43**, 11531 (1991).
[55] G. Ramirez-Santiago and J. V. José, Phys. Rev. Lett. **68**, 1224 (1992); Phys. Rev. B **49**, 9567 (1994); J. V. José and G. Ramirez-Santiago, Phys. Rev. Lett. **77**, 4849 (1996).
[56] Jong-Rim Lee, Phys. Rev. B **49**, 3317 (1994).
[57] Sooyeul Lee and Koo-Chul Lee, Phys. Rev. B **52**, 6706 (1995).
[58] E. Granato, J. M. Kosterlitz, J. Lee, and M. P. Nightingale, Phys. Rev. Lett. **66**, 1090 (1991); J. Lee, J. M. Kosterlitz and E. Granato, Phys. Rev. B **43**, 11531 (1991); J. Lee, E. Granato, and J. M. Kosterlitz, *ibid.* **44**, 4819 (1991); M. P. Nightingale, E. Granato, and J. M. Kosterlitz, *ibid.* **52**, 7402 (1995).
[59] P. Olsson, Phys. Rev. Lett. **75**, 2758 (1995); Phys. Rev. B **55**, 3585 (1997).
[60] E. Granato and D. Dominguez, Europhys. Lett. **63**, 750 (2003); Phys. Rev. B **71**, 094521 (2005).
[61] S. E. Korshunov, Phys. Rev. Lett. **88**, 167007 (2002).
[62] Sun Jon Lee, Jon-Rim Lee, and Bongsoo Kim, Phys. Rev. Lett. **88**, 025701 (2001).
[63] Mahn-Soon Choi, M. Y. Choi, Taesung Choi, and Sung-Ik Lee, Phys. Rev. Lett. **81**, 4240 (1998).
[64] P. W. Anderson, in *Lectures in The Many Body Problem*, edited by E. R. Caianiello (Academic, New York, 1964), Vol. 2.
[65] C. Bruder, R. Fazio, A. Kampf, A. van Otterlo, and G. Shön, Phys. Scr. **42**, 159 (1992).
[66] A. van Otterlo, K. H. Wagenblast, R. Fazio, and G. Shön, Phys. Rev. B **48**, 3316 (1993).
[67] C. Rojas, J. V. José, and A. M. Tikofsky, Bull. Am. Phys. Soc. **40**, 68 (1995).
[68] Ya. M. Blanter and G. Schön, Phys. Rev. B **53**, 14534 (1996).
[69] Ya. M. Blanter, Rosario Fazio, and G. Schön, Nucl. Phys. B (Proc. Suppl.) **58**, 79 (1997).
[70] Mahn-Soo Choi, J. Phys.: Condens. Matter **10**, 9783 (1998).
[71] J. V. José, J. Stat. Phys. **93**, 943 (1998).
[72] G. Ramírez-Santiago and Jorge V. José, Phys. Rev. B **70**, 174516 (2004).
[73] Said Sakhi, Phys. Rev. B **72**, 024520 (2005).
[74] Said Sakhi, Europhys. Lett. **73**, 267 (2006).
[75] Said Sakhi, Phys. Rev. B **73**, 132505 (2006).
[76] J. V. José, L. P. Kadanoff, S. Kirkpatrick, and D. R. Nelson, Phys. Rev. B **16**, 1217 (1977).
[77] H. Kleinert, *Path Integrals in Quantum Mechanics Statistics and Polymer Physics* (World Scientific, Singapore, 1990).
[78] H. Flyvbreg and H. G. Peterson, J. Chem. Phys. **91**, 461 (1989).
[79] P. Minnhagen and P. Olsson, Phys. Scr. **46**, 97 (1992); L. Xu and P. Minnhagen, Physica C **218**, 94 (1993).
[80] V. L. Berezinskii, Zh. Eksp. Teor. Fiz. **61**, 1144 (1971); J. M. Kozterlitz and D. J. Thouless, J. Phys. C **6**, 1181 (1973); J. M. Kozterlitz, J. Phys. C **7**, 1046 (1974).